Bone 120 (2019) 194–203

Contents lists available at ScienceDirect

Bone

journal homepage: www.elsevier.com/locate/bone

Full Length Article

Improved accuracy in the assessment of vertebral cortical thickness by quantitative computed tomography using the Iterative Convolution OptimizatioN (ICON) method

Timo Damm[a,*], Jaime A. Peña[a], Graeme Michael Campbell[b], Jan Bastgen[b,c], Reinhard Barkmann[a], Claus-Christian Glüer[a]

[a] Section Biomedical Imaging, Department of Radiology and Neuroradiology, University Medical Center Schleswig-Holstein, MOIN CC, Am Botansichen Garten 14, 24118 Kiel, Germany
[b] Helmholtz Zentrum Geesthacht, Institute for Materials Research, Max-Planck Straße 1, 21502 Geesthacht, Germany
[c] Section for Trauma Surgery, Lubinus Clinicum for Orthopaedic Surgery and Trauma Surgery, Steenbeeker Weg 25, 24106 Kiel, Germany

ARTICLE INFO

Keywords:
Quantitative computed tomography
Cortical thickness - accuracy
Cortex deconvolution
Bone mineral density profiles

ABSTRACT

Vertebral whole bone strength is substantially affected by cortical bone properties. Disease and therapy may affect cancellous and cortical bone differently. Unlike Dual X-ray Absorptiometry (DXA), Quantitative Computed Tomography (QCT) permits selective assessment of cortical and cancellous bone, but image quality limits the accuracy. We present an image processing method specifically adopted to thin cortices that substantially improves accuracy.

Ten human vertebrae embedded in epoxy resin were imaged using clinical QCT and High-Resolution QCT (HR-QCT) protocols, both acquired on a clinical whole body CT scanner, whereas high resolution peripheral QCT (HR-pQCT) was used as gold standard. Microstructural variables and BMD were calculated using in-house software Structural*Insight* for QCT and HR-QCT and the manufacturer's μCT evaluation software for HR-pQCT. An adjusted measure, a deconvolved cortical thickness (dcCt.Th), corrected for partial volume effects, was derived applying the new Iterative Convolution OptimizatioN (ICON) method.

Direct measurements of cortical thickness (Ct.Th) showed substantial overestimation with mean ± standard deviation of 1.8 ± 0.5 mm for QCT and 1.5 ± 0.3 mm for HR-QCT compared to 0.37 ± 0.07 mm using HR-pQCT. Correlations of both QCT ($r^2 = 0.05$, $p > 0.5$.) and HR-QCT ($r^2 = 0.38$, $p = 0.060$) with the gold standard HR-pQCT were not significant. Also QCT-based BMD and BMC as well as HR-QCT-based BMD did not show a significant correlation with the gold standard approach. Only HR-QCT-based BMC showed a modest correlation ($r^2 = 0.59$, $p = 0.01$) After applying ICON corrections, dcCt.Th resulted in 0.52 ± 0.09 mm for QCT and 0.43 ± 0.07 mm for HR-QCT, both significantly correlated to HR-pQCT ($r^2 = 0.75$, $p = 0.0012$ and $r^2 = 0.93$, $p < 0.0001$, respectively). The average overestimation bias of Ct.Th was reduced from (402 ± 157)% to (45 ± 17)% for QCT and from (330 ± 69)% to (19 ± 8)% for HR-QCT.

Due to inaccurate segmentation uncorrected QCT-based Ct.Th measures as well as BMD and BMC showed no correlation to HR-pQCT and thus such bias cortical data can be misleading. The application of ICON reduced random overestimation bias to about 50 μm and 20 μm for QCT and HR-QCT, respectively, leading to a recovery of a significant correlation with the reference data of HR-pQCT. This reveals the potential for fairly accurate assessment of cortical thickness, allowing to better characterize cortical mechanical competence. These results warrant testing of the performance in vivo.

1. Introduction

Dual X-ray Absorptiometry (DXA) is the accepted clinical standard method for the assessment of bone fragility in osteoporosis. However, bone strength is affected by cancellous and cortical bone and the contributions of these two envelopes cannot be separated by DXA-based assessment of areal bone mineral density (aBMD). This is because the technique does not incorporate a 3D tomographic approach.

* Corresponding author.
E-mail addresses: timo.damm@rad.uni-kiel.de (T. Damm), jaime.pena@rad.uni-kiel.de (J.A. Peña), graeme.campbell@hzg.de (G.M. Campbell), j.bastgen@gmail.com (J. Bastgen), barkmann@rad.uni-kiel.de (R. Barkmann), glueer@rad.uni-kiel.de (C.-C. Glüer).

https://doi.org/10.1016/j.bone.2018.08.024
Received 14 March 2018; Received in revised form 29 August 2018; Accepted 30 August 2018
Available online 08 September 2018

Quantitative Computed Tomography (QCT) on the other hand permits separation of spongiosa and cortex, but the level of accuracy reached in this process strongly depends on the spatial and density resolution of the imaging protocol and on the segmentation procedure applied.

Standard QCT protocols entail imaging and reconstruction with a slice thickness of typically 1-3 mm and an in-plane pixel size of around 0.3 mm. Thus cortical structures, generally not well aligned with voxel borders and appear blurred due to partial volume effects. Moreover, the blurring often extends beyond the next adjacent voxel due to a broad modulation transfer function (MTF) and, in vivo movement artifacts. Therefore vertebral cortical structures with typical thicknesses around 300 μm [1–3] are depicted with apparent thicknesses of around 2 mm on standard QCT axial images. This gives rise to the cortical structure encompassing 5–10 voxels rather than 1–2 voxels. Furthermore, cortical endplates show an apparent thickness of 2-3 mm, depending on the reconstruction increment and reconstructed slice thickness selected in the QCT protocol.

In conjunction with this blurring effect, cortical BMD is grossly underestimated. Vertebral cortical BMD is mostly determined by cortical tissue mineral density (TMD). Fully mineralized cortical bone has a TMD of around 1200 mg calcium hydroxyapatite (mgCaHA/cm3). Lower values are obtained for freshly deposited bone matrix consisting of collagen fibers yet to be mineralized. Old bone has a higher degree of mineralization compared to younger bone. For vertebrae quantitative data of cortical porosity is rare. Ritzel et al. in their detailed histological analysis reported that the cortical structure is mostly lamellar and only few osteonal structures are present [4]. Fazzalari et al. on the other hand, reported porosity levels of around 25% [5]. This level of porosity was obtained from binarized histological sections stained with van Gieson solution.

Due to the limited spatial resolution of CT scanners it is currently not feasible to measure TMD and Co·Po of the vertebral cortex in vivo. The 10% MTF of e.g. the Siemens Somatom 64 scanner used in our study is protocol dependent with a level of about 367 μm (9.3 cycles/cm @ 120 kV, 180 mA, 120 mm FOV, B70 kernel [6]). Even if measured ex vivo with HR-pQCT *like in this study* (Scanco XtremeCT, featuring an MTF of 10% at a distance of < 105 μm), the blurring effects preclude accurate evaluations. This is still the case with the second generation of HR-pQCT systems (Scanco Xtreme CT II, MTF of 10% at a distance of < 58 μm). However, HR-pQCT does permit assessment of cortical measures with much better accuracy compared to clinical CT scanners with 10% MTFs in the range of several hundred micrometers. BMD and BMC results obtained with protocols on clinical CT scanners thus substantially depend on thresholds selected to define the cortical borders: the higher the threshold, the lower the measured BMC and cortical thickness and the higher the measured BMD. BMC in addition strongly depends on bone size (and thus indirectly on body size) and thus interpretation of absolute values is difficult.

It was the aim of this study to develop and test an algorithm, which calculates a single accurate and robust variable that provides a summary measure incorporating BMD (with both TMD and porosity contributions) and cortical thickness. Such a measure should be fairly insensitive to spatial resolution yet provide a mechanically meaningful measure related to bone strength. The key challenge for this approach is to correctly integrate the cortical mineral contributions blurred over several voxels and at the same time separate them from spongiosa and background signals. In addition, bordering structures such as trabecular mineral, fatty marrow of the spongiosa or noise structures outside the vertebral body should not be incorporated. For this summary measure we chose to express results as *effective cortical thickness*. This is the thickness of a plate that would contain the collected BMC as a fully mineralized cortical bone structure (with TMD = BMD = 1200 mg/cm^3). Two different methods, a density weighted as well as a deconvolved cortical thickness, with different degree of sophistication both yielding an estimate of effective cortical thickness were investigated. We compared QCT-based estimates of effective cortical thickness with the corresponding measure assessed by HR-pQCT as the reference method. Given the substantially better spatial resolution of HR-pQCT [7,8] compared to clinical CT scanners, this method represents an appropriate reference method.

By evaluating the level of correlation with the reference method and calculating residual errors relative to the reference method we assessed the performance of the two measures of effective cortical thickness along with the performance of the classical variables BMD and BMC.

2. Materials and methods

2.1. Samples and CT data acquisition

In this study we examined ten excised human vertebrae embedded in an epoxy resin compound. The specimens were obtained from the *Anatomical Institute* of the *Christian-Albrechts-Universtät zu Kiel*, where ethics approval for harvesting the human bones from donors had been obtained from the responsible ethics review committee. Bone marrow was removed from the vertebrae prior to embedding into epoxy resin to prevent bone degradation. The outer shape of the resin was molded in a way that the bones could be smoothly inserted without an air gap into a CT body phantom (Model 4, Simulator for bone mineral analysis, approx. 30 cm wide and 20 cm high, Computerized Imaging Reference Systems, Inc., Norfolk, Virginia, USA).

CT scans were performed according to the protocols summarized in Table 1. The HR-pQCT data was acquired on an XtremeCT I scanner (Scanco Medical AG, Brüttisellen, Switzerland) at the *Osteoporosezentrum Hamburg* (Germany), whereas the standard clinical QCT and advanced HR-QCT protocols were performed on a clinical Siemens Somatom 64 CT scanner (Siemens, Erlangen, Germany) at the *University Hospital Schleswig-Holstein*, *Campus Kiel* (Germany). The difference in image quality is depicted using a representative slice of the 3D dataset (Fig. 1). Subregions of one vertebrae were also scanned on a Viva80 microCT Scanner (Scanco Medical AG) to depict the cortical fine structure.

2.2. Data processing

For the assessment of cortical thickness from QCT and HR-QCT data we used our in-house software Structural*Insight V3.1.7*, which covers the complete CT data workflow consisting of quality assurance, segmentation, registration and quantitative analysis. It has been used and approved within several QCT and HR-QCT studies, e.g. [9–11]. We

Table 1
CT protocol settings for HR-pQCT, HR-QCT and QCT.

	HR-pQCT	HR-QCT	QCT
Device	Scanco Medical XtremeCT	Siemens Somatom 64	
Voxel size in mm^3	0.082 × 0.082 × 0.082	0.156 × 0.156 × 0.300	0.234 × 0.234 × 1.000
Voltage in kV	60	120	120
Exposure in mAs	190	360	100
Reconstruction kernel	standard	B70s	B40s

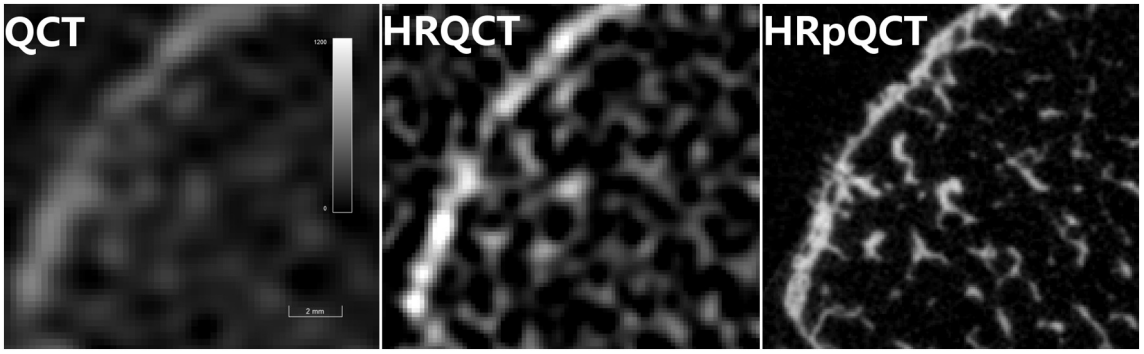

Fig. 1. Slices of registered CT dataset showing a human vertebra's cortical shell imaged at different levels of spatial resolution with associated increasing radiation exposure. From left to right: Standard QCT, High-Resolution QCT HR-QCT and, finally, XtremeCT, usually referred to as High-Resolution peripheral QCT (HR-pQCT).

carried out the following processing steps:

1. *Quality Assurance* by visual inspection of the CT scans prior to study inclusion to select vertebrae without problematic levels of internal gas development and without degenerative cortical structures like large osteophytes.
2. *Calibration* of Hounsfield Units (HU) to mgCaHA/cm^3 using a simultaneously scanned calibration phantom placed below the vertebrae (QRM Model 3 CT Calibration Phantom #2337, QRM GmbH, Möhrendorf, Germany) with density inserts spanning a range of ~ [−50 … 375]mgHA/cm^3. Linear regression was performed to derive the calibration slope and offset.
3. *Template-driven semi-automatic segmentation* of the different volumes of interest (VOI), which include total trabecular volume, ellipse, vertical cortex, upper end plate, lower end plate, and combinations of these VOIs like complete vertebra or complete cortex. The posterior border of the vertebral body was defined by the foramen and by exclusion of the pedicles.

At this point, the segmentation-based cortical thickness (Ct.Th) was calculated (for the vertical cortex only) using the standard *Maximum Sphere* algorithm [12]. *Briefly, in this method the segmentation borders are defined by filling the structure with spheres touching the boundaries. All voxels included in the structure are labeled with the maximum diameter of a sphere centered at the voxel and being contained within the structure*. Besides a simple mean value of these “diameter”-labels two alternative summary measures of effective cortical thickness were obtained:

(I). Density weighted cortical thickness (wCt.Th) obtained by multiplying the “diameter”-labels by BMD/1200 mgCaHA/cm3. For example, a cortex that features an apparent BMD of 600 mgHA/cm^3, which is half the theoretical full mineralization, and a thickness of 2 mm would result in a wCt.Th of 1 mm. According to this approach the blurred shape of the structure in the CT data is considered to be equivalent to a fully mineralized cortex of just 1 mm thickness.

(II). Deconvolution-based cortical thickness (dcCt.Th) was calculated based on the ICON algorithm following these processing steps:

1) Generation of onion-like layers on both sides of the cortical ridge with a constant thickness of 0.2 mm each (see Fig. 2)
2) Calculation of mean BMD within these equidistant layers, referred to as radial BMD.
3) Fitting radial BMD as a function of its distance to the cortical ridge based on a forward modeling approach according to the following steps (for mathematical details compare Appendix A: (De-)convolution-model: mathematical description):
   a) Assuming a Gaussian distribution for the MTF and accordingly for the PSF of the CT imaging system.
   b) Deducing two edge-spread-functions (ESFs), one for the spongiosa plateau and another one for the background level outside the bone, both of which are considered constant and a non-infinitesimal line-spread-function (LSF) for the cortex.
   c) Incorporating these ESFs and the LSF into one combined model.
   d) Setting the full mineralization to 1200 mgHAP/cm^3.
   e) Radial BMD profiles are analyzed, all starting from the center of the vertebra, orthogonally crossing the cortex wall to reach the background outside the bone (epoxy resin). Along these radial paths BMD profiles are fitted to optimally match the BMD levels of the inner spongiosa plateau, at the respective cortex level, and at the background plateau. The blurring caused by the MTF of the imaging system is reflected by a fixed standard deviation (σ).
   f) Obtaining dcCt.Th as one of the four fitting parameters describing the non-linear model (the other three including cortex ridge position, spongiosa plateau mean density and background mean density).

For the HR-pQCT data, we used the μCT manufacturer's software (Scanco μCT_EVALUATION V6.5-3/IPL V5.15, Scanco Medical AG, Brüttisellen, Switzerland). Cortical thickness (based on DT-Tb.Th) within the vertical cortex was calculated based on the *Maximum Sphere* method [12] (this is referred to as the “directly” measured cortical thickness) following well established standards summarized in a consensus paper by Bouxsein et al. [13]. The cortical thickness measured by HR-pQCT on Scanco's XtremeCT 1. Generation has been shown to be highly correlated with MicroCT based data ($r^2 = 0.98$) although the slope slightly deviated from unity, indicating some limits in accuracy [7]. We had to exclude some regions with large osteophytes, because the standard *Maximum Sphere* algorithm is quite sensitive to such structures, because their large local thickness strongly widens the width of the usually thin cortical shell.

For assessment of BMD and BMC, a local relative threshold representing the full-width-at-half-maximum (FWHM), the so called 50% criterion, was applied, similar to the method proposed by Hangartner and Gilsanz [14,15]. Around every mesh point on the cortex a local maximum value is estimated, which is then used to calculate two mesh point-specific density thresholds at 50% of this local maximum: once to the outside at 50% with respect to the background level of the resin and once to the inside at 50% with respect to the average peeled spongiosa BMD. The search for these thresholds was carried out orthogonal to the mesh surface. In contrast to Hangartner and Gilsanz, our segmentation threshold was based on local data rather than on a global maximum cortical density.

2.3. Statistics

Levels of probability of $p < 0.05$ were considered significant. Agreement with HR-pQCT as the reference method was evaluated

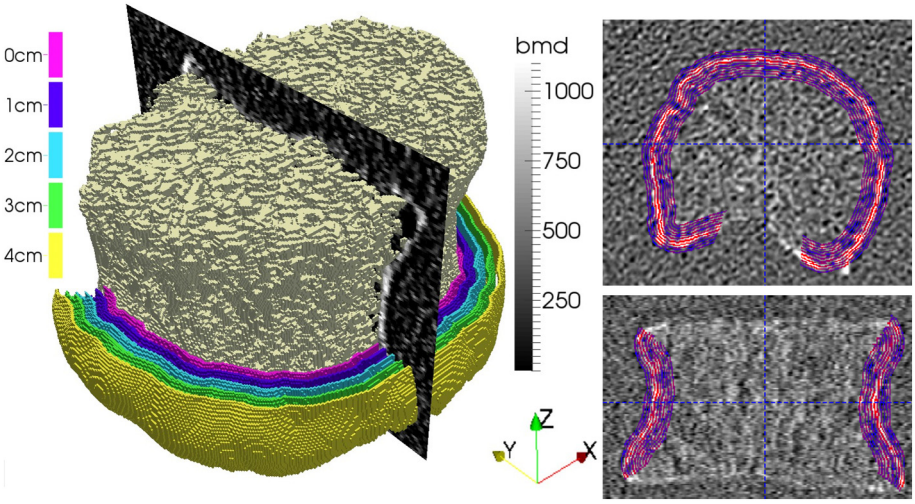

Fig. 2. 3D HR-QCT data of a vertebral body with processes cut off at the pedicles. Left: Every fifth 3D layer is shown; individual layers (width 0.2 mm) are depicted in different colors, the central layer at the cortical ridge at 0 mm is colored in purple. From all layers, the radial mean BMD profile was calculated as a function of the particular layer's distance to the ridge. Layers on the inner side of the ridge are not shown – rather the trabecular bone is depicted in beige color. Cutting this 3D visualization of the vertebral bone centrally, a CT slice of sagittal orientation is depicted showing BMD on a calibrated gray level scale (the corresponding calibration density scale is depicted to the right of the vertebra). Right: Layering scheme for a central axial (right top) and a central coronal (right bottom) 2D section. Each layer has a thickness of 0.2 mm but in order to clarify the visualization these two figure only depict every second layer.

according to a modification of the method of Bland and Altman [16]. All statistical evaluations were performed with JMP 9.0 (SAS Institute, Cary, NC, USA).

3. Results

The fine structure of the cortical shell and its connection to the trabecular network of the spongiosa are visualized in 2D and 3D using µCT (Figs. 3 and 4). The representative images show the cortex as a thin shell of fairly constant thickness, perhaps 3–5 times thicker compared to individual trabeculae. Trabecular struts anchor to this shell attaching it to the spongiosa. These high resolution images of the internal vertebral microstructure supports the rationale of our CT data processing approach, i.e. modeling the cortical shell as a thin plate, that may feature gaps, reducing the TMD level of about 1200 mg CaHAP/cm^3 to the BMD levels observed.

Fig. 5 shows quantitative data of the radial BMD distributions across the cortical shell for the ten specimens investigated. Measured radial BMD profiles are depicted as a function of the ridge distance derived by averaging all voxels of a given layer, i.e. a fixed voxel-to-ridge distance. These profiles were used for fitting the edge- and line-spread functions according to the ICON algorithm. For HR-pQCT scans, we calculated a mean directly measured cortical thickness of 0.37 ± 0.07 mm. For QCT and HR-QCT data, the directly measured Ct.Th of the vertical cortex were 1.78 ± 0.54 mm and 1.53 ± 0.27 mm, respectively. This represents an overestimation of 402% for QCT and 330% for HR-QCT, both relative to HR-pQCT. Ct.Th measured by QCT did not show any correlation with the reference method HR-pQCT ($r^2 = 0.05$, $p = 0.53$) whereas HR-QCT-based Ct.Th showed a weak association just missing significance ($r^2 = 0.38$, $p = 0.06$), see Table 2.

When comparing wCt.Th and dcCt.Th with the reference thickness calculated from HR-pQCT data we have two types of bias: average overestimation and variable residual error. For wCt.Th the average overestimation was reduced by about one order of magnitude and the variable residual error by 70–80%. Application of the ICON algorithm resulted in further reduction of the average overestimation for HR-QCT to a reduction by 94% compared to the directly measured data and it reduced the variable residual error for both QCT and HR-QCT by > 90% compared to the directly measured data. The correlation with the gold standard HR-pQCT-based Ct.Th was recovered by wCt.Th, but even further by dcCt.Th. For QCT a complete lack of correlation ($r^2 = 0.05$) could be recovered to a level of $r^2 = 0.75$. For HR-QCT the improvement led to a change from $r^2 = 0.38$ to $r^2 = 0.93$ (Table 2).

Table 3 presents a similar comparison of QCT and HR-QCT-based estimates of BMD and BMC with the respective values obtained with the reference method HR-pQCT. Due to differences in the segmentation software, the sizes of HR-pQCT and QCT/HR-QCT-based volumes of interest differ and thus comparisons of absolute values are misleading. Therefore for cortical BMC only correlation data are presented. No significant correlation with reference method data was observed for QCT-derived cortical BMC ($r^2 = 0.02$, $p = 0.74$), whereas for HR-QCT-derived cortical BMC, the correlation of $r^2 = 0.59$ was significant at

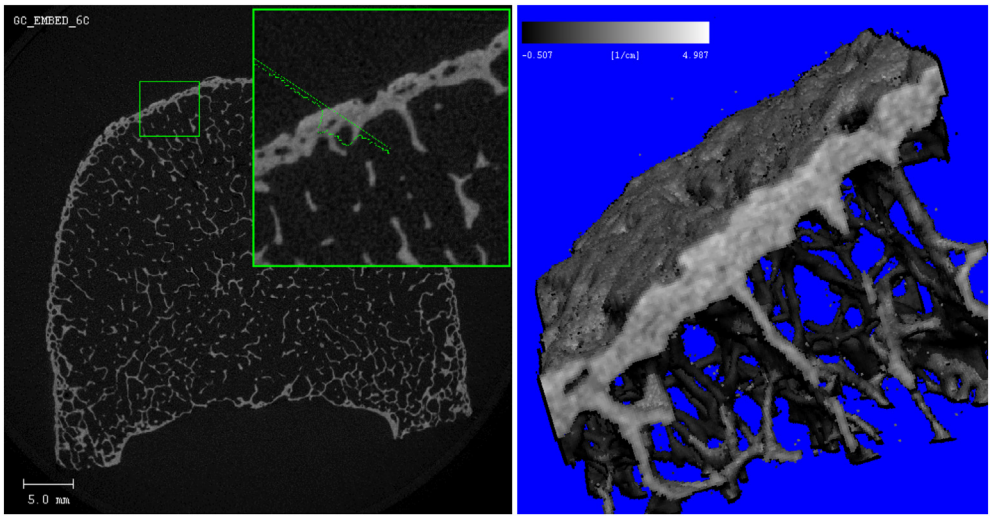

Fig. 3. Representative 2D slice of microCT data from a human vertebra, insert shows enlarged cortical region, depicted in 3D on the right. Within a cortical envelope of approximately 370 µm width (similar to the width measured with HR-pQCT) we observe a peak TMD of up to 1200 mgHA/cm3, an average TMD of 990 mgHA/cm3 and a BMD of 800 mgHA/cm3.

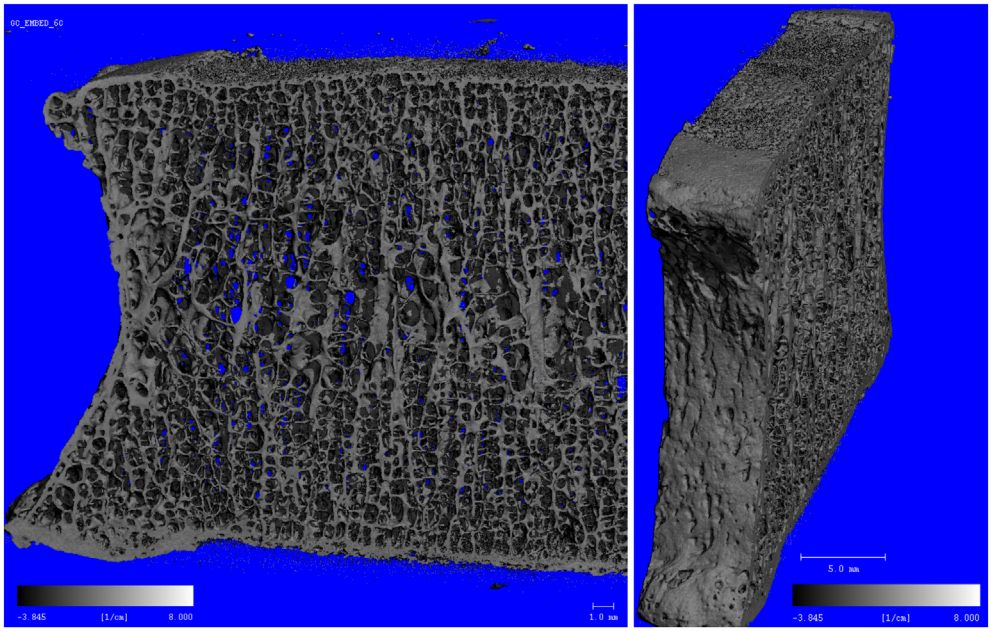

Fig. 4. Representative 3D section of spongiosa and cortex of a human vertebra, shown from two different perspectives.

$p < 0.01$. For cortical BMD, no significant correlation was observed for either technique ($r^2 = 0.02$, $p = 0.71$ for QCT and $r^2 = 0.25$, $p = 0.14$ for HR-QCT).

The Bland-Altman plots presented in Table 4 show the performance of the three cortical variables Ct.Th, wCt.Th, and dcCt.Th for both the HR-QCT and QCT protocols. When compared directly measure Ct.Th data of the reference method HR-pQCT (0.37 ± 0.07 mm, as reported in Table 2) with corresponding QCT HR-QCT data large offsets by > 1.0 mm or 300% are observed for both protocols. These offsets did not show a significant level dependency, although this may in part be due to the large variability of the data. For the two other algorithms the average overestimation is reduced to < 0.14 mm and 0.16 mm for QCT and HR-QCT-based dcCt.Th, respectively. For HR-QCT the ICON method led to a further reduction to around 0.07 mm. The variability of these overestimation errors was also improved: from levels of 0.53 mm and 0.24 mm for QCT and HR-pQCT, respectively, to 0.1 mm and 0.08 mm when determined with wCt.Th for QCT and HR-pQCT, respectively, and further to 50 μm and 20 μm when determined with the ICON algorithm based dcCt.Th for those two CT protocols. The slopes in these diagrams were not significant except for the HR-QCT-based wCt.Th ($p = 0.03$). The residual variability for HR-QCT was substantially smaller compared to QCT (Table 4).

4. Discussion

The ability to separate cortical from cancellous data is a well known hallmark of QCT. DXA does not offer such detail which may be considered as a limitation since it is known that both cancellous and cortical bone contribute to mechanical competence and that drugs may differently affect these two bone envelopes. However, our data document that the limited spatial resolution of standard clinical QCT approaches restrict their ability to accurately differentiate cortical from trabecular bone status. Typical clinical QCT depicts the cortical rim with an apparent thickness close to 2–3 mm along with cortical BMD

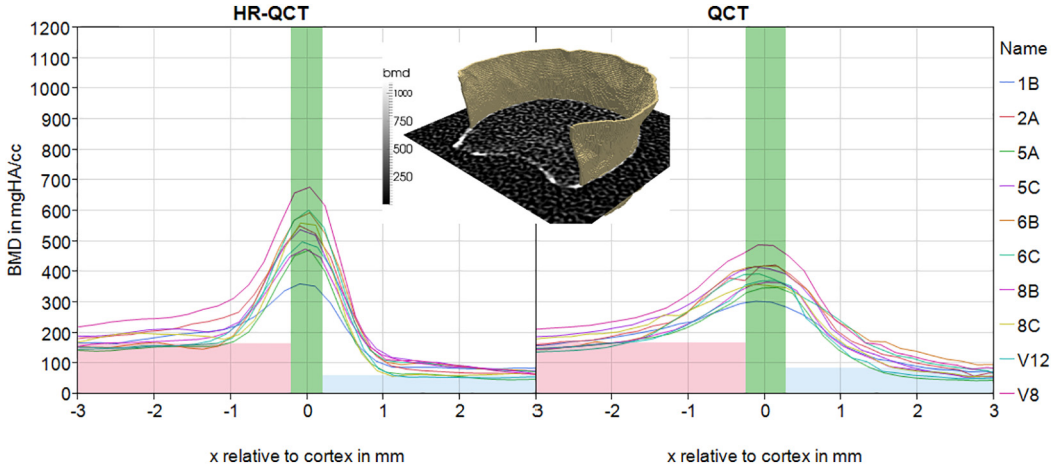

Fig. 5. BMD profiles across the cortical ridge. For each specimen we measured BMD as a function of ridge distance and fitted these profiles according to the ICON algorithm. Three subcompartments of different densities are defined: spongiosa (mean gray rectangles), cortex (central dark gray rectangles), and outer soft tissue (light gray rectangles). Left image: BMD profile according to HR-QCT data, which is less blurred and reaches a higher maximum in comparison to the QCT data BMD profile on the right image. The widths of the central rectangles corresponds to our dcCt.Th estimates. The center 3D insert displays the resulting vertical cortex with deconvolved cortical width calculated according to the ICON algorithm based on HR-QCT data; QCT-based deconvolved cortical width would look similar.

Table 2
Estimates of cortical thickness by QCT and HR-QCT, and compared to the gold standard HR-pQCT (means ± standard deviation), the last column depicts the correlation between HR-pQCT and QCT or HR-QCT, respectively.

Variable	CT method	Mean ± SD	Overestimation absolute data	Overestimation [%]	Correlation [r^2]
Ct.Th [mm]	HR-pQCT	0.37 ± 0.07			
	QCT	1.78 ± 0.54	1.42 ± 0.53	402 ± 157	0.05
	HR-QCT	1.53 ± 0.27	1.17 ± 0.24	330 ± 69	0.38***
wCt.Th [mm]	QCT	0.50 ± 0.14	0.14 ± 0.10	39 ± 27	0.49*
	HR-QCT	0.52 ± 0.13	0.16 ± 0.08	44 ± 19	0.74**
dcCt.Th [mm]	QCT	0.52 ± 0.09	0.16 ± 0.05	45 ± 17	0.75**
	HR-QCT	0.43 ± 0.07	0.07 ± 0.02	19 ± 8	0.93****

* $p < 0.05$.
** $p < 0.01$.
*** $p < 0.001$.
**** $p < 0.0001$.

values ranging around 200–300 mgHA/cm^3 [9,17], substantially less than the true level of TMD of around 1200 mgHA/cm^3 [18–20]. In this study, for standard QCT similar results were observed but even more disconcerting there was no significant correlation of cortical thickness, BMD or BMC with the respective measures obtained by our reference technique HR-pQCT. Therefore, it is questionable whether standard QCT-based cortical BMD, BMC and thickness measurements carry meaningful clinical information about bone status. Even for the higher dose approach of HR-QCT no significant correlation for BMD was evident. At least for BMC, the HR-QCT data led to a significant, but still weak correlation ($r^2 = 0.59$, $p = 0.009$).

In order to improve the accuracy of cortical measurements we developed an image processing techniques that largely corrects the bias introduced by limited spatial resolution. As a basis for developing this correction algorithm we had to obtain an accurate understanding of the 3D geometry of the vertebral cortical shell. This could then be used to model the impact of partial volume effects and the MTF on QCT measurements of the cortex.

Cortical thickness measurements have been assessed in early studies in the 1990s. Using histological methods, i.e. microscopy on sections of bone, Ritzel and colleagues showed that cortical thickness ranges between 200 and 400 µm in healthy individuals. With aging cortical thickness decrease by 50–100 µm and in osteoporosis it is reduced to levels mostly between 150 and 250 µm [4].

3D electron microscopy images from Alan Boyde's group show an even more extreme situation: the cortical shell is similar in thickness to trabecular plates and somewhat thicker than trabecular struts [21]. In fact the structure depicted in virtually all of the cases in this paper depicts vertebral bodies almost completely made up of trabecular bone with an outer layer of thin cortical bone that looks equally thin, the only difference being that the cortical shell is formed like a plate where the trabecular, at least in the elderly, are showing the typical rod-like structure.

These observations formed the basis for our modeling approach: cortical bone as a thin plate of bone with a TMD of about 1200 mgCaHA/cm^3 but with some gap or pores that reduce the measured cortical BMD of this plate. We reaffirmed this model by obtaining 3D µCT images of the cortical shell as shown in Figs. 3 and 4. The age and osteoporosis related loss of cortical mass thus is likely to follow a pattern that differs from the one observed for the femoral neck, which has received a lot of research attention in recent years [22]. The cortical shell of vertebrae is too thin to undergo a pattern of trabecularization like that one observed on thick parts of the proximal femur, in the calcar region [23], where, in contrast to the vertebral cortex, the subsegmentation of the femoral cortex [24] is a useful approach. There is a fairly clear cut inner boundary of the plate and trabecular struts connect to this inner surface to stabilize the vertebral-cortical interface structure. With osteoporosis fewer and fewer struts connect and thus larger parts of the cortical shell remains unsupported, and are thus more likely to cave. This leads to the pattern of endplate deformation typical for osteoporotic fracture.

Our image-processing model thus was based on this 3D geometry of a thin cortical shell of fairly constant thickness made up of bone mineral with a TMD of 1200 mgHA/cm^3. We investigated two approaches of different complexity to characterize cortical mineral status. The simpler approach, density weighted cortical thickness (wCt.Th), already showed substantial improvements compared to the directly measured Ct.Th. However, in contrast to ICON's dcCt.Th, this algorithm is still affected by selection of the segmentation borders, which are noise dependent, as they rely on a 50% thresholding criterion in our case (mean value between the cortex ridge density and the cancellous density on the inside or the resin/soft tissue background density on the outside). Especially for QCT, this cut-off is not very robust, as a great portion of the cortex's signal is mapped to regions outside this segmentation due to the poor MTF. Also, for cortical thickness levels below the full width half maximum (FWHM) of the LSF of the scanner/kernel combination,

Table 3
Results of cortical BMD and BMC based on QCT and HR-QCT, and compared to the gold standard HR-pQCT (means ± standard deviation). The last column depicts the correlation between HR-pQCT and QCT or HR-QCT, respectively.

Variable	Method	Mean ± SD	Underestimation	Underestimation [%]	Correlation [r^2]
BMD [mgHA/cm^3]	HR-pQCT	504.4 ± 64.9	–	–	–
	QCT	315.4 ± 57.9	189.0 ± 81.0	37 ± 13	0.02*
	HR-QCT	405.6 ± 59.1	89.8 ± 62.2	19 ± 11	0.25***
BMC [mgHA]	HR-pQCT	360.3 ± 107.8	–	–	–
	QCT	1092.1 ± 414.6	NA[a]	NA[a]	0.02****
	HR-QCT	1339.8 ± 256.3	NA[a]	NA[a]	0.59**

* $p < 0.05$.
** $p < 0.01$.
*** $p < 0.001$.
**** $p < 0.0001$.
[a] due to partially different segmentation methods and VOI sizes of HR-pQCT and QCT/HR-QCT.

Table 4
Bland-Altman plots of HR-QCT and QCT variables versus the gold standard HR-pQCT value. Dashed lines represent 95% confidence interval of the linear fit.

	HR-QCT	QCT
Ct.Th	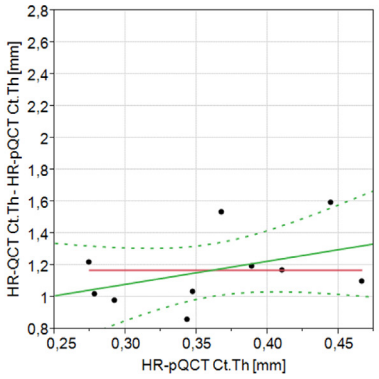	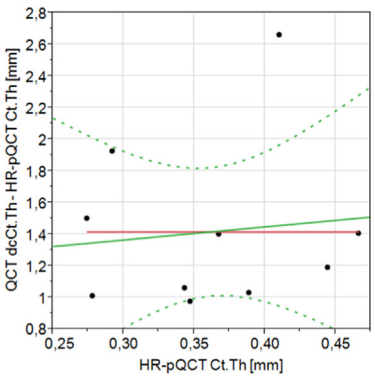
wCt.Th	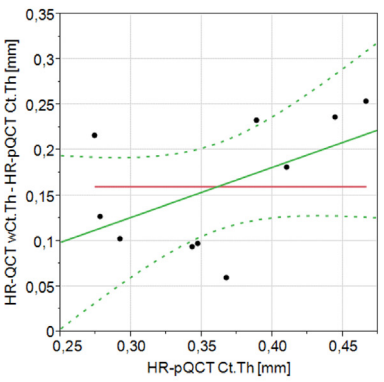	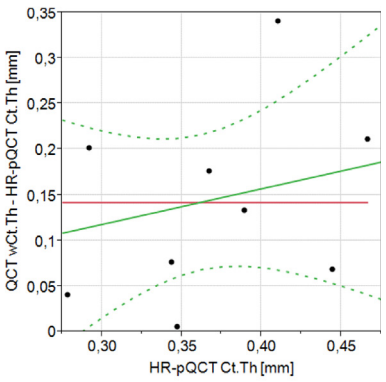
dcCt.Th	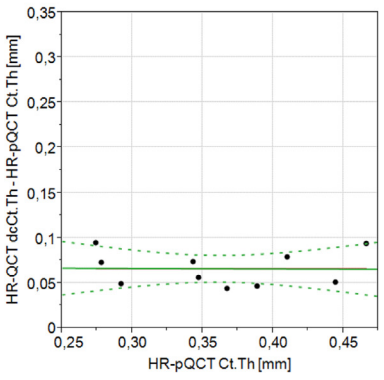	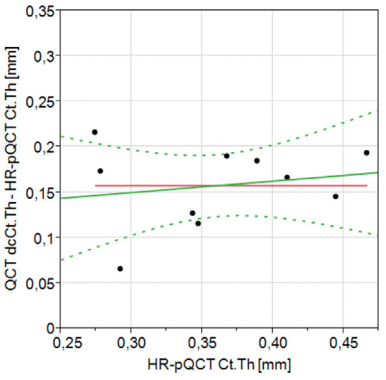

the accuracy is limited [25], what is very obvious particularly for the standard QCT protocol with its coarse spatial resolution.

In order to maximize the ability to accurately characterize cortical bone status and to develop a robust measure, the advanced concept of the ICON algorithm showed clear advantages over wCt.Th. This concept is characterized by the following assumptions: plate-like structure of the cortical shell, TMD of 1200 mgHA/cm^3, zero porosity. In other words, we calculate the thickness of a truly compact cortex of TMD = 1200 mgHA/cm^3. Density profile across (i.e. orthogonal to) the cortical shell was modeled on the basis of a three component structure. The cortical shell encloses the spongiosa characterized by the average cancellous BMD. On its outer side, the cortical shell is surrounded by external tissue (soft tissue in vivo/resin for our excised vertebral specimen), the density of which can be measured very accurately. The levels of the cortex signal outside the cortical boundaries and the density signals in the cortex originating from the spongiosa and the soft tissue can be determined using the ICON fitting procedure, utilizing the ESF and the LSF as manifestations of the cortex model chosen. The result is a model of a compact cortical plate with an effective cortical thickness characterized by dcCt.Th. Of note, the ICON procedure does not require explicit input of the LSF but can optimize the fit accordingly. In fact, using a free σ, the outlined fit procedure can be used to roughly access the systems imaging quality by turning the vertebra's cortex itself into a “test body” to access the PSF's FWHM.

Rather than determining the thickness of the cortex in a mapping procedure for every subarea of the cortical plate we average the density

values in equidistant "onion-like" layers parallel to the cortical plate. This results in a substantial improvement in robustness and reduction of noise since density levels are averaged over millions of voxels for each layer. This allows the generation of a very accurate profile of the average radial density distribution, perpendicular to the cortical plate. Moreover, the hypothetical mineral content of the resulting LSF/ESF solution equals the mineral present within the complete cortical region investigated in contrast to single-position fitting strategies.

The results of our study demonstrate that the resulting cortical measure dcCt.Th has a number of strong performance characteristics: the measure correlates highly with the reference method HR-pQCT derived measure (r^2 = 93% for HR-QCT and 75% for QCT) with average accuracy error offsets of 19% and 45% for HR-QCT and QCT, respectively. These average accuracy errors could be largely reduced by standardization: for a given scanner our set of vertebrae could be scanned in a similar fashion as in this paper and from the resulting model fit the scanner specific correction algorithm could be derived. The remaining variable residual random accuracy errors of 5% and 11% for HR-QCT and QCT, respectively, correspond to around 20–50 μm, excellent levels considering the thickness of only 250–400 μm of the cortical shell and the limits of spatial resolution. It could only be achieved due to the average across millions of voxels in the equidistant layers. With this magnitude it should be possible to study treatment effects of bone anabolic medications since the treatment effect is on the same order of magnitude. Of note, for QCT dcCt.Th but not wCt.Th provided high correlation with the reference method. For HR-QCT the ultimate level of performance with a small residual random error and virtually no dependency on the level of the gold standard-based cortical thickness was achieved, a strong indication that this approach does yield robust estimates.

In many studies BMC as an integral of BMD across cortical bone volume has been used because, similar to density weighted cortical thickness, this measure also integrates BMD and thickness and thus partially overcomes the limitations of spatial resolution. However, our data indicate a lack of correlation with the reference method and thus the use of BMC appears questionable, at least for standard QCT. The lack of correlation may in part be due to our limited sample size. But since our ICON-based thickness measure showed a highly significant correlation with the reference method despite the limited sample size, dcCt.Th appears to be a more robust measure compared to BMC.

Similar approaches for improved assessment of cortical thickness have been investigated by other groups. A method using analytical models to describe the imaging system's blur has been previously reported by Prevral et al. [25,26]. Another method to calculate a corrected cortical thickness using a point-wise mapping approach was described and further refined by Treece et al. [27–29]. The algorithm published by these authors involved collecting voxels in an arbitrary, local neighborhood of rays localized on the cortex with perpendicular alignment. In contrast to their method, ICON is based on a computationally fast distance transform on the complete segmentation, and averages all voxels within a defined distance range to form the radial BMD density profiles.

Treece and colleagues investigated the femoral cortex aiming to calculate thickness maps around the complete proximal femur. Because of the variable orientation of the cortical surface of different parts of the proximal femur in their setting, the correction of the crude out-of-plane resolution is crucial and they have to calculate profiles at every point of their map. They claim to independently measure the femoral cortical thickness and the cortical mineralization [28]. This becomes possible to some degree with the thicker cortex of the femur but remains very challenging on thinner cortices. Also the issue of ambiguity of the inner cortical boundary at the femoral neck has to be taken into consideration.

Our approach and the study have limitations. Most importantly, the performance of the ICON algorithm so far was only tested on specimen ex vivo. The limited sample size was sufficient to develop and test the method but it requires confirmation on larger data sets, preferably in vivo. However, in vivo there is no gold standard method available that could be used to directly measure the method's accuracy. Therefore, validation would have to be investigated indirectly, by checking whether use of dcCt.Th would improve performance on patients, i.e. with regard to fracture discrimination or differentiation of treatment effects. We did confirm the convergence of the algorithm on in vivo CT data and have initiated first analyses on patient data to be analyzed in another publication. Second, our gold-standard method HR-pQCT, while offering much higher spatial resolution compared to clinical CT scanners, does not have perfect accuracy on thin structures like vertebral cortices, and thus we may underestimate accuracy errors.

The locally derived 50% criterion used to segment the cortex yields larger results for cortical thicknesses compared to using a higher threshold based on the global maximum cortical density described by Hangartner and Gilsanz [14,15]. However, the results for density weighted cortical thickness should be similar since the differences in measured thickness and density are in opposite directions and thus should largely balance. However, for ICON, such a potential bias should be of lesser importance, since only the outer segmentation border serves as a starting reference. Since we average out results for the entire vertical cortex we assume that the outcome is more robust compared to calculations based on a global maximum cortical density.

As our QRM Model 3 CT Calibration Phantom is made for standard clinical CT protocols it does not contain inserts with density higher than 375 mgHA/cm^3. Within the density range covered the relationship of CT numbers versus BMD is linear with typical coefficients of correlation of $r^2 > 0.999$, but some uncertainty regarding linearity at higher densities for the HR-QCT protocol remains.

The ICON approach does not produce a map of cortical thickness. We did not pursue this goal because our main focus was on deriving a measure that can be used to assess average changes in effective cortical thickness as a function of disease or treatment. In such longitudinal studies, scanner specific differences in spatial resolution or patient related differences in noise level (e.g. due to body size and obesity) will be limited given the typical time courses of a year or two. The algorithm separating the cancellous and the external soft tissue compartment is also appropriately set up to distinguish between endosteal and periosteal changes, an aspect of substantial interest for the assessment of the mechanism of new bone anabolic medications, specifically with regard to their biomechanical impact.

In reality, the shape of the profiles reflects not only thickness of the cortex, but also the mineralization state of the cortex and its porosity. And both parameters most probably vary along the profile to some degree, which may be affected by age, health, dietary habits and medication. As long as the resolution cannot be reduced well below the thickness of the structure of interest, these internal structures have to be neglected, as we did in the proposed model of a compacted cortex used in the ICON algorithm. And due to the partial volume effect, the level of porosity within the structure is not measurable until we can actually image these small pores.

Another aspect is the anisotropy of spatial resolution, which is very significant using a standard QCT protocol: in-plane (x,y) we typically have resolution levels of 0.2 mm–0.4 mm, but out-of-plane (i.e. in the axial direction z), due to the sampling and also the underlying slice thickness, it is usually in the range of 1 mm to 3 mm. To avoid distortions by this crude resolution, we evaluated the cortex just in its vertical portion, where due to the positioning of the samples (and patients laying along the scanner's z-axis) our profiles are mostly impacted by the higher in-plane resolution. For measurements of T12, our preferred choice for patient studies, the long axis of the vertebra is typically well aligned with the long-axis of the scanner.

There are interesting perspectives for further refinements of the approach. While we concentrated on the vertical cortex the same approach can be implemented for the endplates, although here the challenges of spatial resolution and complexity due to near-neighborhood

features such as intervertebral disks are higher. While we explicitly aimed to derive a single measure of cortical status, under certain assumptions one could incorporate the impact of temporal changes in TMD and/or porosity. Assuming that changes in these two aspects are largely governed by systemic factors affecting bone turnover, one could potentially measure porosity and/or TMD on peripheral bones, where techniques with better spatial resolution are available with the assumption that changes at all cortical sites are to some extent correlated. Thus dcCt.Th could then be adjusted based on peripheral TMD or porosity data, in effect refining the level of 1200 mgCaHA/cm^3. We also could try to produce cortical thickness maps based on the ICON algorithm, and, taking this one step further, to reprocess the 3D image of the vertebrae, replacing the blurred cortex with a deconvolved thin high density cortex. Such a reprocessed image could be used as a basis for finite element modeling, potentially permitting more accurate modeling of fracture processes. Creating a network of appropriately shaped elements that truly reflect the thinness of the vertebral cortex should yield more accurate estimates of vertebral whole bone strength under different loading conditions.

In conclusion, deconvolution-based estimation of cortical thickness using the ICON algorithm reduces the huge overestimation of cortical thickness from over 300% for both QCT and HR-QCT to 19% (HR-QCT) and 45% (QCT) with low residual random accuracy errors. Whereas cortical thickness and BMD or BMC of standard QCT did not provide meaningful information about true cortical status, using ICON a very high correlation of cortical thickness with the gold standard could be achieved. Of note, while best performance was achieved for HR-QCT (r^2 = 0.93****), a good performance was also achieved for regular QCT (r^2 = 0.75**), an important aspect for limiting radiation exposure. Interpretation of BMC was just useful for HR-QCT (r^2 = 0.59**).

Our results warrant application of the ICON algorithm in clinical CT studies. In this initial limited sample of embedded vertebral bodies, ICON-based Ct.Th appears to be more accurately reflecting cortical properties than cortical BMD or BMC. Assuming that a more accurate depiction of cortical thickness will improve the ability to model bone fragility using finite element models, the ICON method may serve to improve image quality and thus data accuracy required for mechanical modeling. Due to its robust averaging across layers parallel to the cortical ridge the method can also be applied in longitudinal treatment studies in disease or to assess the effect of treatment on strengthening the cortical shell.

Acknowledgement

Dr. med. Isolde Frieling supported the XtremeCT scans at the Osteoporosezentrum Hamburg. We also like to acknowledge our former group members Sonja Waldhausen, who did the QCT and HRQCT scans, as well as Wolframm Timm, Christian Graeff and Felix Thomsen, who were former developers of Structural*Insight*. This work was in part supported by the Grant No. 01EC1005 of the German Federal Ministry of Education and Research (BMBF).

Appendix A. (De-)convolution-model: mathematical description

A.1. Rationale and concept

Image convolution is a standard approach for modeling spatial resolution in the context of the imaging process [30]. The dataset is folded with a kernel functional by means of spatial integration. A Gaussian functional is commonly used to model the blurring caused by limited spatial resolution incorporating also noise. For CT data, filter kernel differ for in-plane variations versus those observed in the z-direction. In single-slice CT, one could use a step function in z-direction, but considering commonly available fan-beam and helical CT data, this simplification is not justified anymore.

The ICON method developed for improving blurring effects in CT imaging of bone is based on a deconvolution approach, in which the convolution effects during data acquisition are estimated and corrected for. In this appendix we describe the different parts of our convolution kernel, used to generate a combined filter, which in turn was used in a standard nonlinear solver (JMP 9.0, SAS Institute, Cary, NC, USA) to estimate the model parameters of the modeling process that describes the imaging process. This solving process can be considered as a deconvolution, as we backwards calculate the imaging process. Direct deconvolution of 2D/3D data suffers from substantial sensitivity to noise leading to instability. Our method, which is iterative in nature, is very stable, as it works on the averaged data of our radial density distributions calculated for an initial 3D segmentation. Constraining the combined filter to the assumed model of the spongiosa-cortex-soft tissue background complex further stabilizes the procedure.

Appendix B. Mathematical modeling

B.1. Point Spread Function (PSF) and image convolution

We assume a Gaussian imaging filter kernel. As we work just on the vertical cortex, the complex 3D problem is reduced to 2D:

$$PSF(x,y,\sigma) = \frac{e^{-\frac{x^2+y^2}{2\sigma^2}}}{2\pi\sigma^2}$$

with in-plane coordinates x and y and the variance σ^2, where the full-width-half maximum $FWHM(\sigma) is given as\ 2\sqrt{2\sigma^2 \bullet ln\,2} \approx 2.355 \bullet \sigma$.

Following the approach reported by Prevral [25], the radially symmetric σ is assumed to define the complete imaging process (performance depending on scanner type, scan protocol and CT reconstruction kernel). The process of image convolution to transfer the object geometry into the resulting CT data is derived by integration:

$$CT\ Data\ (x,y) = \iint BMD\_Model(x,y) \bullet PSF(x-x', y-y')dx'dy'$$

B.2. Edge Spread Function (ESF)

Similarly, the Edge Spread Function (ESF) used to model one side of an infinite wide step function:

$$ESF\ (x,y,\sigma,bmd,x_0) = \int_{-\infty}^{x_0}\int_{-\infty}^{+\infty} bmd \bullet PSF\,(x-x',y-y')dx'dy'$$

with constant density plateau height *bmd* and step position x_0 being deduced by convolution. In our model it was used to model the influence of the mean BMD of the spongiosa inside the vertebrae, which, after convolution, also spreads into the cortex region and generates even a shift of the radial density distribution peaks inwards. Another ESF has been used to model the soft tissue signal from outside the vertebra.

B.3. Line Spread Function (LSF)

To model the thin cortex of width *d*, a similar convolution was made to deduce the Line Spread Function (LSF) as follows:

$$\mathrm{LSF}\ (x,y,\sigma,bmd_{full},x_0,w) = \int_{x_0}^{x_0+w}\int_{-\infty}^{+\infty} bmd_{full} \bullet PSF\,(x-x',y-y')dx'dy'$$

with constant $bmd_{full} = 1200\,\mathrm{mgHA/cm^3}$, center position x_0 and width *w*.

B.4. Combined Model

To apply a single function to the collected radial density distribution of the ICON method, we just had to combine one LSF reflecting the cortex with two ESF for the bones interior trabecular network and the soft tissue outside the bone with adopted parameters to form a continuous model of the assumed bone profile.

$$\begin{aligned}\mathrm{Combined\ Model}(\sigma,bmd_{spongiosa},bmd_{full},bmd_{soft\_tissue},x_0,w) = {} & ESF_{Spongiosa}\,(\sigma,bmd_{spongiosa},x_0) + LSF_{Cortex}\,(\sigma,bmd_{full},x_0,w)\\ & + ESF_{Soft\_Tissue}\,(\sigma,bmd_{soft\_tissue},x_0+w)\end{aligned}$$

Using this combined model in in a numerical solver, e.g. nonlinear fit of JMP 9.0 (SAS Institute, Cary, NC, USA), using fixed σ and bmd_{full}, the remaining four parameters $bmd_{spongiosa}$, bmd_{sost_fissue}, endosteal cortex edge x_0 and width *w*, referred to as dcCt.Th in this paper, can be solved at once. Due to the pronounced profile shape after averaging the data in the layers, this solving procedure is very stable.

We are open to share the code of the ICON method with interested researchers.

References

[1] M.J. Silva, C. Wang, T.M. Keaveny, W.C. Hayes, Direct and computed tomography thickness measurements of the human, lumbar vertebral shell and endplate, Bone 15 (4) (1994) 409–414.

[2] A. Vesterby, L. Mosekilde, H.J. Gundersen, F. Melsen, L. Mosekilde, K. Holme, S. Sorensen, Biologically meaningful determinants of the in vitro strength of lumbar vertebrae, Bone 12 (3) (1991) 219–224.

[3] W.J. Whitehouse, E.D. Dyson, C.K. Jackson, The scanning electron microscope in studies of trabecular bone from a human vertebral body, J. Anat. 108 (Pt 3) (1971) 481–496.

[4] H. Ritzel, M. Amling, M. Posl, M. Hahn, G. Delling, The thickness of human vertebral cortical bone and its changes in aging and osteoporosis: a histomorphometric analysis of the complete spinal column from thirty-seven autopsy specimens, J. Bone Miner. Res. 12 (1) (1997) 89–95.

[5] N.L. Fazzalari, I.H. Parkinson, Q.A. Fogg, P. Sutton-Smith, Antero-postero differences in cortical thickness and cortical porosity of T12 to L5 vertebral bodies, Joint Bone Spine 73 (3) (2006) 293–297.

[6] N. Keat, D. Platten, D. Lewis, S. Edyvean, Siemens Somatom Sensation Open CT Scanner Technical Evaluation, NHS – Purchasing and Supply Agency, Centre for Evidence-Based Purchasing, London, 2005.

[7] J.A. MacNeil, S.K. Boyd, Accuracy of high-resolution peripheral quantitative computed tomography for measurement of bone quality, Med. Eng. Phys. 29 (10) (2007) 1096–1105.

[8] K. Sekhon, G.J. Kazakia, A.J. Burghardt, B. Hermannsson, S. Majumdar, Accuracy of volumetric bone mineral density measurement in high-resolution peripheral quantitative computed tomography, Bone 45 (3) (2009) 473–479.

[9] C.C. Glüer, F. Marin, J.D. Ringe, F. Hawkins, R. Moricke, N. Papaioannu, P. Farahmand, S. Minisola, G. Martinez, J.M. Nolla, C. Niedhart, N. Guanabens, R. Nuti, E. Martin-Mola, F. Thomasius, G. Kapetanos, J. Pena, C. Graeff, H. Petto, B. Sanz, A. Reisinger, P.K. Zysset, Comparative effects of teriparatide and risedronate in glucocorticoid-induced osteoporosis in men: 18-month results of the EuroGIOPs trial, J. Bone Miner. Res. 28 (6) (2013) 1355–1368.

[10] C. Graeff, G.M. Campbell, J. Pena, J. Borggrefe, D. Padhi, A. Kaufman, S. Chang, C. Libanati, C.C. Gluer, Administration of romosozumab improves vertebral trabecular and cortical bone as assessed with quantitative computed tomography and finite element analysis, Bone 81 (2015) 364–369.

[11] C. Graeff, F. Marin, H. Petto, O. Kayser, A. Reisinger, J. Pena, P. Zysset, C.C. Gluer, High resolution quantitative computed tomography-based assessment of trabecular microstructure and strength estimates by finite-element analysis of the spine, but not DXA, reflects vertebral fracture status in men with glucocorticoid-induced osteoporosis, Bone 52 (2) (2013) 568–577.

[12] T. Hildebrand, P. Rüegsegger, A new method for the model-independent assessment of thickness in three-dimensional images, J. Microsc. 185 (1) (1997) 67–75.

[13] M.L. Bouxsein, S.K. Boyd, B.A. Christiansen, R.E. Guldberg, K.J. Jepsen, R. Muller, Guidelines for assessment of bone microstructure in rodents using micro-computed tomography, J. Bone Miner. Res. 25 (7) (2010) 1468–1486.

[14] T.N. Hangartner, Thresholding technique for accurate analysis of density and geometry in QCT, pQCT and microCT images, J. Musculoskelet. Neuronal Interact. 7 (1) (2007) 9–16.

[15] T.N. Hangartner, V. Gilsanz, Evaluation of cortical bone by computed tomography, J. Bone Miner. Res. 11 (10) (1996) 1518–1525.

[16] J.S. Krouwer, Why Bland-Altman plots should use X, not (Y + X)/2 when X is a reference method, Stat. Med. 27 (5) (2008) 778–780.

[17] T.F. Lang, J. Li, S.T. Harris, H.K. Genant, Assessment of vertebral bone mineral density using volumetric quantitative CT, J. Comput. Assist. Tomogr. 23 (1) (1999) 130–137.

[18] G.J. Kazakia, A.J. Burghardt, T.M. Link, S. Majumdar, Variations in morphological and biomechanical indices at the distal radius in subjects with identical BMD, J. Biomech. 44 (2) (2011) 257–266.

[19] A. Laib, H.J. Hauselmann, P. Ruegsegger, In vivo high resolution 3D-QCT of the human forearm, Technol. Health Care 6 (5–6) (1998) 329–337.

[20] A.M. Laval-Jeantet, C. Bergot, R. Carroll, F. Garcia-Schaefer, Cortical bone senescence and mineral bone density of the humerus, Calcif. Tissue Int. 35 (3) (1983) 268–272.

[21] J.A. Jayasinghe, S.J. Jones, A. Boyde, Three-dimensional photographic study of cancellous bone in human fourth lumbar vertebral bodies, Anat. Embryol. (Berl) 189 (3) (1994) 259–274.

[22] M.E. Kersh, M.G. Pandy, Q.M. Bui, A.C. Jones, C.H. Arns, M.A. Knackstedt, E. Seeman, R.M. Zebaze, The heterogeneity in femoral neck structure and strength, J. Bone Miner. Res. 28 (5) (2013) 1022–1028.

[23] W.J. Whitehouse, E.D. Dyson, Scanning electron microscope studies of trabecular bone in the proximal end of the human femur, J. Anat. 118 (Pt 3) (1974) 417–444.

[24] R. Zebaze, A. Ghasem-Zadeh, A. Mbala, E. Seeman, A new method of segmentation of compact-appearing, transitional and trabecular compartments and quantification of cortical porosity from high resolution peripheral quantitative computed tomographic images, Bone 54 (1) (2013) 8–20.

[25] S. Prevrhal, K. Engelke, W.A. Kalender, Accuracy limits for the determination of cortical width and density: the influence of object size and CT imaging parameters, Phys. Med. Biol. 44 (3) (1999) 751–764.

[26] S. Prevrhal, J.C. Fox, J.A. Shepherd, H.K. Genant, Accuracy of CT-based thickness measurement of thin structures: modeling of limited spatial resolution in all three dimensions, Med. Phys. 30 (1) (2003) 1–8.

[27] G.M. Treece, A.H. Gee, Independent measurement of femoral cortical thickness and cortical bone density using clinical CT, Med. Image Anal. 20 (1) (2015) 249–264.

[28] G.M. Treece, A.H. Gee, P.M. Mayhew, K.E. Poole, High resolution cortical bone thickness measurement from clinical CT data, Med. Image Anal. 14 (3) (2010) 276–290.

[29] G.M. Treece, K.E. Poole, A.H. Gee, Imaging the femoral cortex: thickness, density and mass from clinical CT, Med. Image Anal. 16 (5) (2012) 952–965.

[30] W. Birkfellner, Applied medical image Processing: A Basic Course, Taylor & Francis Publishers, Boca Raton, FL, USA, 2010.